Geoinformation for European-wide Integration, Benes (ed.)

A new tool for measuring terrain deformation evolution by means of Synthetic Aperture Radar interferometry

P. Berardino, G. Fornaro, R. Lanari & E. Sansosti
IREA-CNR, via Diocleziano 328, 80124 Napoli, Italy

Keywords: interferometry, Synthetic Aperture Radar, ground deformation

ABSTRACT: A new approach for the evaluation of Earth surface deformation *evolution* based on an easy and effective combination of low baseline DIFSAR interferograms is presented. The proposed solution extends a least-squares interferogram combination technique already presented in the literature via the application of the Singular Value Decomposition (SVD) method and satisfies two key requirements: to increase the "temporal sampling rate" by using all the available acquisitions and to retain the areal information relative to the detected deformations, which is a key issue of conventional DIFSAR interferometry. The capability of the proposed approach to follow the dynamics of the detected deformations has been fully demonstrated by using data acquired in the time interval 1992-2000 by the European Remote Sensing (ERS) satellites and relative to the Campi Flegrei area (Italy).

1 INTRODUCTION

Differential Synthetic Aperture Radar Interferometry (DIFSAR) is a relatively new technique that has been successfully used for generating large-scale surface deformation maps on a dense grid (the displacement field being measured in the radar line of sight) and with a centimeter to millimeter accuracy. While the DIFSAR approach has been applied several times to the analysis of a single deformation episode (Massonnet *et al.*, 1993; Massonnet *et al.*, 1995; Peltzer and Rosen, 1995; Rignot, 1998; Stramondo *et al.*, 1999; Borgia *et al.*, 2000), the interest of the scientific community is now progressively moving towards the study of the temporal evolution of the detected deformations and some results have already been presented (Vadon and Sigmundsson, 1997; Lanari *et al.*, 1998; Tesauro *et al.*, 2000; Lundgren *et al.*, 2001; Usai, 2000; Berardino *et al.*, 2001).

An effective way to study the temporal behavior of the detected phenomena is the generation of time-series that allows us to follow the evolution of the monitored deformations; to do this, the information available from each data pair must be properly related to those included in the other acquisitions via the generation of an appropriate sequence of DIFSAR interferograms. A key limitation, in this case, is that data pairs used to generate differential interferograms must be acquired from relatively close tracks (the spatial separation between orbits is referred to as *baseline*) in order to reduce both spatial decorrelation and topography errors. In practical cases, as for the ERS-1/2 sensors, the available acquisitions are generally distributed in Small Baseline (SB) subsets, separated by large "baselines"; accordingly, only one deformation time series for each subset can be easily obtained (Lundgren *et al.*, 2001; Usai, 2000). Since these results are typically poorly sampled in time and not linkable to those computed from other subsets, the limitation to exploit all the available acquisitions for the generation of an overall deformation time-series is evident.

Some advances in this field have been recently introduced at the expenses of the processed area coverage. First of all, it has been demonstrated that small manmade features remain very correlated over time (Usai and Klees, 1999; Usai, 2000), although interferograms over these areas only show pointwise information. Moreover, a new solution for maximizing the number of used acquisitions has been proposed and it is referred to as Permanent Scatterers (PS) technique (Ferretti *et al.*, 2000; Ferretti *et al.*, 2001). This approach implies the generation, with respect to a common (master) image, of a DIFSAR interferogram for each available acquisition even if the exploited data pair is characterized by a large baseline (even larger than the critical baseline) and therefore affected by baseline decorrelation phenomena. It is evident that, in this case, the

use of all the available data acquisitions is accomplished, but at the imaged pixel density expenses; indeed, only those targets that exhibit sufficiently high coherence values, even at large spatial baselines (i.e., the PS targets) are considered and their density may be, in some cases, rather low; this often happens, for instance, in non-urban areas.

This work proposes a new DIFSAR approach for the evaluation of the Earth surface deformation *evolution;* it extends the technique presented by Lundgren *et al.* (2001) and Usai (2001) to the case of multiple SB acquisition subsets via an easy and effective combination of all the available SB interferograms. The combination is based on a minimum norm criterion of the velocity deformation, easily obtained in our case via the application of the Singular Value Decomposition (SVD) method. The presented technique satisfies two key requirements: to increase the "temporal sampling rate" by using all the acquisitions included in the different SB subsets and to preserve the capabilities of the system to provide spatially dense deformation maps, which is a key issue of conventional DIFSAR interferometry. Clearly, the latter requirement is related to the use of small baseline interferograms that limit the baseline decorrelation phenomena. We further remark that our approach is easily implemented as a post-processing step applied to the set of DIFSAR interferograms that may be generated via already available interferometric data processing tools.

The proposed combination technique relies on the use of unwrapped DIFSAR interferograms, with the unwrapping operation implemented via sparse-grid approach (Costantini and Rosen, 1999). Moreover, in spite of the limited influence of possible errors in the removal of the topographic phase contribution, an estimate of the topography error is included in our processing algorithm to increase its robustness. Additionally, an atmospheric phase artifacts filtering operation is carried out on the obtained space-time deformation measurements following the lines of the solution developed for the PS technique; in our case the filtering operation takes benefit from the high spatial density of the imaged pixels.

Presented results, obtained on the data acquired in the time interval 1992-2000 by the European Remote Sensing (ERS) satellites and relative to the Campi Flegrei caldera and to the city of Napoli (Italy), demonstrate the capability of the proposed approach to follow the dynamic of the detected deformations.

2 PROBLEM FORMULATION

Let us start our analysis by considering *N+1* SAR images relative to the same area and acquired at the ordered times $(t_0,....,t_N)$. We also assume that each acquisition may interfere with at least another image; this implies that each SB subset is composed by a minimum of two acquisitions. Based on the above hypothesis we conclude that the number of possible differential interferograms, say *M*, satisfies the following inequality[1]:

$$\frac{N+1}{2} \le M \le \frac{N}{2}(N+1) \quad . \tag{1}$$

Consider now the generic *j*-interferogram computed, in the pixel of azimuth and range coordinates (x,r), from the SAR acquisitions at times t_B and t_A; this, following the topographic phase component removal, is given by:

$$\delta\phi_j(x,r) = \phi(t_B,x,r) - \phi(t_A,x,r) \approx \frac{4\pi}{\lambda}\left[d(t_B,x,r) - d(t_A,x,r)\right] \quad , \tag{2}$$

wherein λ is the transmitted signal central wavelength and $d(t_B,x,r)$ and $d(t_A,x,r)$ are the line of sight (LOS) cumulative deformations at times t_A and t_B with respect to the instant t_0, assumed as a reference. As a consequence, we have that $d(t_0,x,r) \equiv 0$ and therefore it is natural to identify $d(t_i,x,r)$, with $i = 1,..,N$, as the wanted deformation time series and to assume $\phi(t_i,x,r)$ as the associated phase component, thus $\phi(t_i,x,r) \approx 4\pi\, d(t_i,x,r)/\lambda$.

A few additional remarks on eq. (2) are in order. First of all we note that in the equation the decorrelation phenomena have been totally neglected as well as possible phase artifacts caused by changes in the atmosphere refraction index between the acquisitions and/or due to a non precise removal of the topographic phase component; these assumptions allow us to simplify the presented analysis without losing the rationale of the discussion and will be removed in the next section.

Moreover, we have also implicitly assumed that the phase signal is unwrapped and calibrated with respect to one pixel whose deformation is known (typically a high coherent pixel located in a non-deforming zone). A further feature of the proposed technique implies a pixel-by-pixel temporal analysis; accordingly, the dependence of eq. (2) on the (x,r) variables is not explicitly mentioned hereafter. Let:

$$\boldsymbol{\phi}^{\mathrm{T}} = [\phi(t_1),\ldots,\phi(t_N)] \tag{3}$$

be the vector of the *N* unknown phase values associated with the deformation of the considered pixel and:

$$\boldsymbol{\delta\phi}^{\mathrm{T}} = [\delta\phi_1,\ldots,\delta\phi_M] \tag{4}$$

be the vector of the *M* (known) values of the computed DIFSAR interferograms. Eq. (4) identifies the following two index vectors:

[1] We have implicitly assumed *N* odd.

$$IS = [IS_1,\ldots,IS_M],\quad IE = [IE_1,\ldots,IE_M]; \tag{5}$$

corresponding to the acquisition time-indexes associated with the image pairs used for the interferogram generation. Note also that we assume the master (*IE*) and slave (*IS*) images to be chronologically ordered, i.e., $IE_j > IS_j \ \ \forall j = 1,\ldots,M$. In other words we have that:

$$\delta\phi_j = \phi(t_{IE_j}) - \phi(t_{IS_j}) \qquad \forall j = 1,\ldots,M. \tag{6}$$

Accordingly, the expression (6) defines a system of *M* equations in *N* unknowns that may be organized in the following matrix representation:

$$\mathbf{A}\boldsymbol{\phi} = \boldsymbol{\delta\phi} \tag{7}$$

being $\mathbf{A}$ an $M \times N$ matrix where $\forall j = 1,\ldots,M$ we have: $A(j, IS_j) = -1$ if $IS_j \neq 0$, $A(j, IE_j) = +1$ and 0 otherwise. For instance, should be $\delta\phi_1 = \phi_4 - \phi_2$ and $\delta\phi_2 = \phi_3 - \phi_0$, $\mathbf{A}$ would have the following form:

$$\mathbf{A} = \begin{bmatrix} 0 & -1 & 0 & +1 & \ldots \\ 0 & 0 & +1 & 0 & \ldots \\ \ldots & \ldots & \ldots & \ldots & \ldots \\ \ldots & \ldots & \ldots & \ldots & \ldots \end{bmatrix} \tag{8}$$

Equation (8) highlights that $\mathbf{A}$ is an incidence-like matrix, directly depending on the set of interferograms generated from the available data. Due to this characteristic, if all the acquisitions belong to a single SB subset it turns out that $M \geq N$ and $\mathbf{A}$ is an *N-rank* matrix. Accordingly, the system of equations (7) is a well- ($M = N$) or an over-determined ($M > N$) system and its solution can be obtained, in general, in the LS sense as (Strang, 1988):

$$\hat{\boldsymbol{\phi}} = \mathbf{A}^{\#}\boldsymbol{\delta\phi} \qquad \mathbf{A}^{\#} = \left(\mathbf{A}^{\mathrm{T}}\mathbf{A}\right)^{-1}\mathbf{A}^{\mathrm{T}} \tag{9}$$

Unfortunately, as pointed out in the previous section, the availability of an entire data set belonging to a single SB subset is typically uncommon; therefore, in order to increase the temporal sampling rate of the deformation signal, we must face the case of data belonging to different subsets. Clearly, we might still refer to the formulation in (7), but it is easily recognized that in this case $\mathbf{A}$ exhibits a rank deficiency and therefore $\mathbf{A}^{\mathrm{T}}\mathbf{A}$ is a singular matrix in eq. (9). For instance, if we assume to face *L* different SB subsets, the rank of $\mathbf{A}$ will be *N-L+1* and the system will have infinite solutions.

A simple solution for inverting the system in (7) is provided by the SVD method (Strang, 1988). This allows us to evaluate the pseudo-inverse of the matrix $\mathbf{A}$ which gives the minimum norm LS solution of the system of equations (7).

In particular, by using the "thin SVD decomposition" (Golub and van Loan, 1996), we decompose $\mathbf{A}$ as follows:

$$\mathbf{A} = \mathbf{U}\mathbf{S}\mathbf{V}^{\mathrm{T}} \tag{10}$$

where $\mathbf{U}$ is an orthogonal $M \times M$ matrix whose columns, called the left-singular vectors of $\mathbf{A}$, are the eigenvectors of $\mathbf{A}\mathbf{A}^{\mathrm{T}}$; $\mathbf{V}$ is an orthogonal $N \times M$ matrix whose columns, the right-singular vectors of $\mathbf{A}$, are the eigenvectors of $\mathbf{A}^{\mathrm{T}}\mathbf{A}$ and $\mathbf{S}$ is the $M \times M$ matrix whose entries (the singular values σ_i) are the square root of the corresponding eigenvalues of the $M \times M$ matrix $\mathbf{A}\mathbf{A}^{\mathrm{T}}$. Being generally *M>N*, *M-N* eigenvalues are zero; moreover, due to the singular nature of $\mathbf{A}$ there are *L-1* additional null eigenvalues. In summary we have:

$$\mathbf{S} = \mathrm{diag}(\sigma_1,.....,\sigma_{N-L+1},0,...0). \tag{11}$$

The estimate $\boldsymbol{\phi}$ in the LS sense with minimum norm is finally obtained as follows:

$$\hat{\boldsymbol{\phi}} = \mathbf{A}^{+}\boldsymbol{\delta\phi} \qquad \mathbf{A}^{+} = \mathbf{V}\mathbf{S}^{+}\mathbf{U}^{\mathrm{T}}$$
$$\mathbf{S}^{+} = \mathrm{diag}(1/\sigma_1,.....,1/\sigma_{N-L+1},0,...0) \tag{12}$$

that is:

$$\hat{\boldsymbol{\phi}} = \sum_{i=1}^{N-L+1} \frac{\boldsymbol{\delta\phi}^T\mathbf{u}_i}{\sigma_i}\mathbf{v}_i \quad . \tag{13}$$

where $\mathbf{u}_i$ and $\mathbf{v}_i$ are the column vectors of $\mathbf{U}$ and $\mathbf{V}$, respectively.

This solution is characterized by a minimum norm constraint on the phase signal and, accordingly, on the detected deformation, see (2). As a consequence, the method forces the solution, in accordance with the starting equation system (7), to be as close to zero as possible. Unfortunately, this solution method may introduce large discontinuities in the cumulative deformations obtained, thus leading to a physically meaningless result.

In order to guarantee a physically sound solution, we manipulate the equation system in (7) in such a way to replace the unknowns with the mean phase velocity between time adjacent acquisitions. Accordingly, the new unknowns become:

$$\underline{v}^T = \left[v_1 = \frac{\phi_1}{t_1 - t_0} \quad , \quad \ldots. \quad , \quad v_N = \frac{\phi_N - \phi_{N-1}}{t_N - t_{N-1}} \right] \tag{14}$$

and, in place of (6), we have:

$$\sum_{k=IS_j}^{IE_j-1} (t_{k+1} - t_k)\, v_k = \delta\phi_j, \ \forall j = 1,\ldots,M \tag{15}$$

that, organized in a matrix form, finally leads to the expression:

$$\mathbf{B}\mathbf{v} = \boldsymbol{\delta\phi}. \tag{16}$$

Note that the matrix $\mathbf{B}$ is again an $M \times N$ matrix; however, we have now that the generic (j,k) element will be $B(j,k) = t_{k+1} - t_k$ for $IS_j \leq k \leq IE_j$ $\forall\ j = 1,\ldots,M$, and $B(j,k) = 0$ elsewhere. Of course,

in this case the SVD decomposition is applied to the matrix **B** and the minimum norm constraint for the velocity vector **v** does not imply the presence of large discontinuities in the final solution; obviously, an additional integration step is necessary to achieve the final solution $\boldsymbol{\phi}$.

3 PROCESSING ALGORITHM

Before going in the details of the algorithm implementing the SVD-based approach discussed in the previous section, it is important to reconsider, in a more realistic scenario, the DIFSAR phase expression in eq. (2); accordingly, let us rewrite the interferometric signal as follows:

$$\begin{aligned}\delta\phi_j(x,r) &= \phi(t_B,x,r)-\phi(t_A,x,r)\approx \\ &\frac{4\pi}{\lambda}\left[d(t_B,x,r)-d(t_A,x,r)\right]+\frac{4\pi}{\lambda}\frac{B_{\perp j}\,\Delta z}{r\sin\vartheta} \\ &+\left[\phi_{atm}(t_B,x,r)-\phi_{atm}(t_A,x,r)\right]+\Delta n_j \\ &\forall j=1,\ldots,M\end{aligned} \qquad (17)$$

wherein three additional phase components, with respect to eq. (2), are present.

The first additional term accounts for possible phase artifacts caused, within the DIFSAR phase generation process, by an error Δz in the knowledge of the scene topography; note that the impact of these artifacts depends on the orbit separation component $B_{\perp j}$ (usually referred to as perpendicular baseline or simply baseline) as well as on the sensor target distance r and on the look angle ϑ. The second one accounts for possible atmospheric inhomogeneities between the acquisitions at times t_A and t_B and it is often referred to as atmospheric phase component. Finally, the term Δn_j accounts for phase contributions caused by the baseline and temporal decorrelation phenomena and by the thermal noise effects.

In addition to the above, in a real case, only the restriction to the $(-\pi,\pi)$ interval of the interferometric phase (wrapped phase) is directly measurable from the registered image pairs; therefore, since equation (16) relies on the availability of unwrapped signals, a retrieval operation must be carried out on the wrapped data. It is important to underline that the unwrapping operation is applied to each DIFSAR phase pattern but only involves those pixels that exhibit an estimated coherence value higher than an assumed threshold; this hypothesis allows us to exclude the pixels strongly affected by noise that, therefore, carry out no significant phase information and may have a negative impact on the performance of the unwrapping procedure. In particular, we have implemented the approach presented in (Costantini and Rosen, 1999) which is suitable for such a kind of sparsely coherent data.

After the phase unwrapping, the application of the SVD method described in the last section would lead to the computation of the unknown velocity vector. However, we usually perform a joint estimation of this unknown vector and of the topographic error Δz (see eq. 17) through the SVD inversion of the following equation:

$$[\mathbf{B},\mathbf{c}]\mathbf{a}=\boldsymbol{\delta\phi}$$

$$\text{wherein}\quad \mathbf{c}^T=\left[\frac{4\pi}{\lambda}\frac{B_{\perp 1}}{r\sin\vartheta},\ldots\ldots,\frac{4\pi}{\lambda}\frac{B_{\perp M}}{r\sin\vartheta}\right] \qquad (18)$$

$$\text{and}\quad \mathbf{a}^T=\left[\mathbf{v}^T,\Delta z\right].$$

Even if the need for the estimation of the topographic factor Δz in (18) could appear irrelevant due the hypothesis of low baseline interferograms, we remark that the amplitude of local topographic artifacts may significantly exceed the expected DEM accuracy, thus causing a remarkable degradation of the produced DIFSAR fringes

Finally, a trivial integration step leads us to the measurement of the phase signal $\phi(t_i,x,r)\ \forall t_i$ with *i=1,...,N*.

However, in view of eq. (17), it is evident that the results obtained does not only account for the wanted deformation signal $d(t_i,x,r)$ but also for the decorrelation effects and for possible topographic and atmospheric artifacts.

As far as the decorrelation phenomena are concerned, we remark that they are significantly mitigated by the complex multilook operation carried out within the DIFSAR interferograms generation process and by the coherence-driven pixels selection; moreover, also the effect of possible topographic artifacts is drastically reduced following their detection based on eq. (18).

On the contrary, the presence of an atmospheric phase component represents a critical issue because it may significantly reduce the accuracy of the detected deformations and, in some case, completely mask them out (Goldstein, 1995; Tarayare and Massonnet, 1996; Zebker *et al.*, 1997). Therefore, in order to mitigate the effect of these atmospheric artifacts, a filtering operation must be performed on the output of the SVD-based procedure. In this case the applied filtering operation is derived from the PS approach (Ferretti *et al.*, 2000; Ferretti *et al.*, 2001) which is based on the observation that the atmospheric signal phase component is characterized by a high spatial-correlation but exhibits a significantly low temporal-correlation.

Once the atmospheric phase component has been evaluated, it is finally subtracted from the estimated phase signal; the conversion into a displacement signal is eventually achieved via the multiplication by the correction factor $\lambda/4\pi$, see eq. (17).

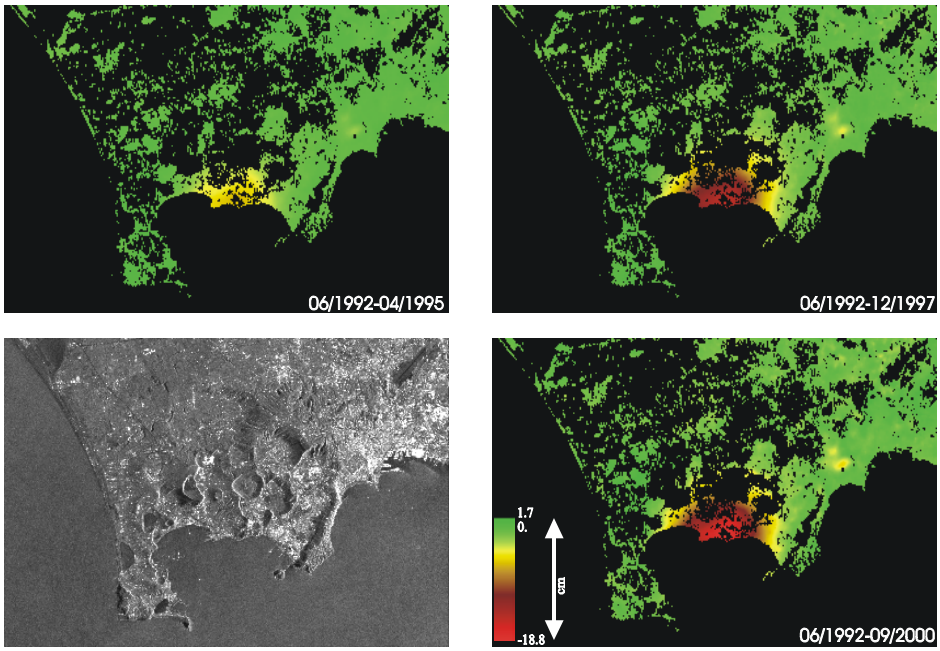

Figure 1. Temporal evolution of the deformation measured in the time interval 06/1992 – 04/1995, 06/1992 – 12/1997 and 06/1992 – 09/2000; The SAR image of the observed area is also included (bottom left) to simplify the identification of deforming zones. Black areas represent zones where no reliable deformation signal is available.

4 RESULTS

The validation of the presented approach has been carried out by using an ERS-1/ERS-2 data set composed by 44 acquisitions acquired, from 08/06/1992 until 28/09/2000, on a descending orbit and distributed in three small baseline subsets; the 70 DIFSAR interferograms used in this study are characterized by a (perpendicular) baseline value smaller than 130 m.

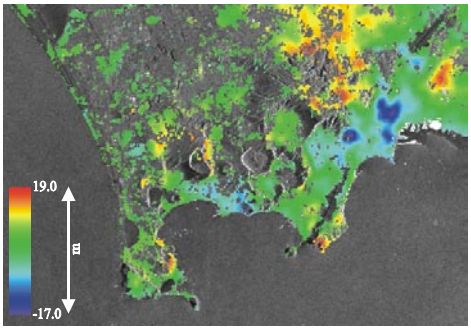

Figure 2. False color map of the detected topography errors superimposed on the SAR image amplitude of the investigated area

The test site, located in southern Italy, includes the active caldera of Campi Flegrei and the city of Napoli (see Fig. 1 – bottom left). The overall analysis has been carried out on DIFSAR products obtained following a complex multilook operation with 4 looks in the range direction and 20 in the azimuth one; hence, the pixel dimension is about $85\times80m$ in azimuth and range directions, respectively; moreover, the coherence threshold has been fixed to 0.25. We remark that the pixel dimensions have been chosen rather large in order to map significantly wide areas without drastically expanding the overall amount of data; moreover, the large number of complex looks also allows us to reduce the phase noise. Figure 1 shows the temporal evolution of the deformation measured in the time interval 06/1992 – 04/1995, 06/1992 – 12/1997 and 06/1992 – 09/2000, respectively.

The topographic phase component has been removed by using a DEM provided by the Italian Army, whose nominal height accuracy is about 10 to 20 m, and the ERS-1/ERS-2 precise orbit state vectors computed by the Technical University of Delft. In this case, despite the expected accuracy, significant topography artifacts have been detected, see Fig. 2, thus making the refined topography phase removal operation a relevant step. Note also that the presented approach is applied to pixels exhibiting an

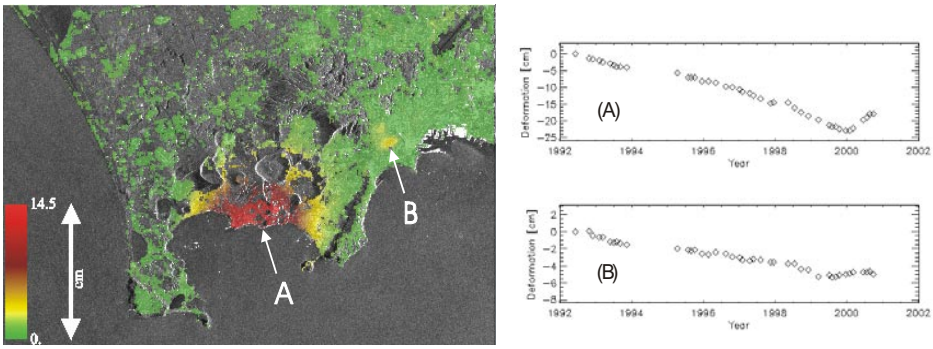

Figure 3. False color map of the measured deformation *rms* superimposed on the SAR image amplitude of the investigated area. The temporal evolution of the deformations in the selected points identified by A and B are also shown.

estimated coherence value higher than the selected threshold in at least 30% of the computed interferograms. This assumption is consistent with the chosen strategy of maximizing the spatial information.

In order to provide an overall picture of the detected deformation, we present in Fig. 3 the false color map representing the root mean square (*rms*) value of the computed deformation, for each investigated pixel, superimposed on the gray-scale representation of the SAR image amplitude. Note that this *rms* representation is visually effective and allows us to provide, for each pixel of the investigated area, an integral information (with respect to time) of the detected deformation whose amount becomes more significant as we move from green areas (stable zones) to red ones (highly deforming zones); obviously, areas where the measurement accuracy is affected by decorrelation noise have been excluded from the false color map.

Fig. 3 clearly shows that a significant deformation pattern is present in two areas which can be easily identified: the largest one, on the left hand side, represents the Campi Flegrei caldera while the one on the right side, significantly smaller, is located in the Vomero zone, a densely populated quarter within the city of Napoli. In order to demonstrate the capability of the proposed approach to follow the temporal evolution of the detected deformation, some examples are provided. The point marked by A is located in the area of maximum subsidence/uplift of the Campi Flegrei caldera and is characterized by a rather continuous subsidence phenomenon from 1992 until the beginning of 2000, when a change of the deformation trend occurs resulting in an uplift phase. The deformation of the area marked by B was originally revealed by DIFSAR techniques (Tesauro *et al.*, 2000); however, the presented technique allows us not only to identify the occurring deformations but also to track their temporal evolution, as evident by considering the temporal plot of Fig. 3.

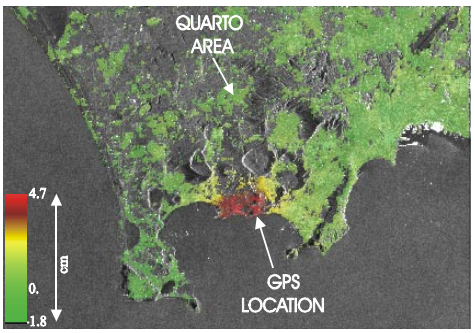

Figure 4. Deformation map relative to the time interval 3/2000 – 9/2000. In the area of maximum deformation the GPS measures a deformation (projected along the SAR line of sight) of 4.14 cm, while we measure 4.05 cm. Both measurements are referred to the Quarto area assumed stable.

These results are confirmed by geodetic measurements carried out by the researchers of the Osservatorio Vesuviano (OV), which is the institution in charge of monitoring the deformations occurring in the area. In particular, due to the availability of differential GPS measurements performed during the uplift crisis[2] of the year 2000, it was possible to perform a comparison between the SAR results and the geodetic measurements carried out in March and September 2000 in the points indicated by arrows in Fig. 4. The results obtained by projecting, in the radar line of site, the GPS measurement performed in the area of maximum deformation (relative to Quarto area) gives 4.14 cm of displacement whereas the corresponding SAR measurement results in 4.05 cm; the good agreement between the two different types of data is evident.

Unfortunately, no geodetic measurements were available in the Vomero area and therefore no comparison was possible.

[2] These data have a height accuracy of about 1cm (Osservatorio Vesuviano, 2000).

As a final remark, we note that the presented technique has been also successfully applied to study the deformations occurring at the Vesuvius volcano (Lanari *et al.*, 2002).

5 CONCLUSIONS

This paper describes an innovative technique for investigating surface deformations via the Differential Interferometric SAR technique. This approach is based on the use of a large number of SAR acquisition distributed in Small Baseline subsets; it allows the easy combination of DIFSAR interferograms computed via standard processing techniques and computation of a time sequence of the deformation.

Key features of the proposed techniques are the large number of useful SAR data acquisitions, that allows to increase of the temporal sampling rate of the monitoring, and the high degree of spatial coverage over the area of interest, related to the use of small baseline interferograms only.

The technique we present is applied pixel-by-pixel to all the areas exhibiting a sufficiently high coherence degree and is robust with respect to possible errors of the Digital Elevation Model used in the derivation of the differential interferograms. Moreover, the availability of both time and space information, allows us to effectively remove the atmospheric artifacts in the results via a proper space-time filtering operation. More sophisticated, or even optimal, atmospheric filtering techniques could be included in the processing algorithm and can be the object of further developments.

Since it is based on a simple inversion of a linear model, it is intrinsically plausible to introduce an a-priory knowledge about the temporal behavior of the deformation into the technique. Moreover, an easy extension of this model to pixel groups, or even to the whole available areas, allows us to benefit from the introduction of 3D, space-time, deformation models.

As a final remark we underline that the proposed technique is not suitable, at the present stage, for detecting local deformations on a small spatial scale as, for example, in the case of small buildings suffering a structural stress; however, the extension of our approach to the detection and monitoring of such local deformation seems rather simple and preliminary results on these issues look very promising (Mora *et al.*, 2002).

ACKNOWLEDGMENTS

This work has been partially sponsored by the Italian Space Agency, by the European Space Agency and by the (Italian) National Group for Volcanology (GNV). The DEM of the area has been provided by the I.G.M. of the Italian Army and the precise ERS-1/ERS-2 satellite orbit state vectors by the Technical University of Delft, The Netherlands. We also want to thank S. Usai for interesting discussions, J. Bequignon for his support, and P. De Martino and G. P. Ricciardi for providing us with GPS measurements of the Campi Flegrei area.

REFERENCES

Berardino, P., G. Fornaro, A. Fusco, D. Galluzzo, R. Lanari, E. Sansosti and S. Usai, 2001. A new Approach for Analyzing the Temporal Evolution of Earth Surface Deformations based on the Combination of DIFSAR Interferograms. *Proceedings of International Geoscience and Remote Sensing Symposium (IGARSS 2001)*, Vol. 6: 2551 –2553.

Berardino, P., G. Fornaro, R. Lanari and E. Sansosti, 2002. A new Algorithm for Surface Deformation Monitoring based on Small Baseline Differential SAR Interferograms, *IEEE Transactions on Geoscience and Remote Sensing*, to appear.

Borgia, A. , R. Lanari, E. Sansosti, M. Tesauro, P. Berardino, G. Fornaro, M. Neri and J. Murray, 2000. Actively growing anticlines beneath Catania from the distal motion of Mount Etna's decollement measured by SAR interferometry and GPS. *Geophysical Research Letters*, Vol. 27 (No. 20): 3409-3412.

Costantini, M. and P. A. Rosen, 1999. A generalized phase unwrapping approach for sparse data. *Proceedings of International Geoscience and Remote Sensing Symposium (IGARSS 1999)*, Vol. 1: 267–269.

Ferretti, A. , C. Prati, F Rocca, 2000. Nonlinear subsidence rate estimation using permanent scatterers in differential SAR interferometry. *IEEE Transactions on Geoscience and Remote Sensing*, Vol. 38 (No. 5): 2202–2212.

Ferretti, A. , C. Prati, F Rocca, 2001. Permanent scatterers in SAR interferometry. *IEEE Transactions on Geoscience and Remote Sensing*, Vol. 39 (No.1): 8–20.

Franceschetti, G. and G. Fornaro, 1999. *Synthetic Aperture Radar Interferometry*, Chapter 4 in G. Franceschetti and R. Lanari, *Synthetic Aperture Radar Processing*, Boca Raton, FL: CRC-PRESS.

Goldstein, R. M. , 1995. Atmospheric limitations to repeat-track radar interferometry. *Geophysical Research Letters*, Vol. 22: 2517-2520.

Golub, G. H. and C. F. Van Loan, 1996. *Matrix computation*. Baltimore: Johns Hopkins University Press.

Lanari, R. , P. Lundgren and E. Sansosti, 1998. Dynamic Deformation of Etna Volcano Observed by Satellite Radar Interferometry. *Geophysical Research Letters*, Vol. 25 (No. 10): 1541-1544.

Lanari, R., G. De Natale, P. Berardino, E. Sansosti, G. P. Ricciardi, S. Borgstrom, P. Capuano, F. Pingue and C. Troise, 2002. Evidence for a peculiar style of ground deformation inferred at Vesuvius volcano. *Geophysical Research Letters*, to appear.

Lundgren, P. , S. Usai, E. Sansosti, R. Lanari, M. Tesauro, G. Fornaro and P. Berardino, 2001. Modeling Surface Deformation observed with SAR Interferometry at Campi Flegrei Caldera. *Journal of Geophysical Research*, Vol. 106 (No. B9): 19,355-19,367.

Massonnet, D. , M. Rossi, C. Carmona, F. Ardagna, G. Peltzer, K. Feigl and T. Rabaute, 1993. The displacement field of the Landers earthquake mapped by radar interferometry. *Nature*, Vol. 364: 138-142

Massonnet, D. , P. Briole, A. Arnaud, 1995. Deflation of Mount Etna Monitored by Spaceborne Radar Interferometry. *Nature*, Vol. 375: 567-570.

Mora, O., R. Lanari, J. J. Mallorquí, P. Berardino and E. Sansosti, 2002. A New Algorithm for Monitoring Localized Deformation Phenomena Based on Small Baseline Differential SAR Interferograms. *Proceedings of International Geoscience and Remote Sensing Symposium (IGARSS 2002)*, to appear.

Osservatorio Vesuviano, 2000. Crisi bradisismica della Caldera dei Campi Flegrei 2000 (in Italian), Internal Report.

Peltzer, G. and P. A. Rosen, 1995. Surface Displacement of the 17 May 1993 Eureka Valley, California, earthquake observed by SAR interferometry. *Science*, Vol. 268: 1333-1336,.

Rignot, E., 1998. Fast recession of a west Antarctic glacier, *Science*, Vol. 281: 549-551.

Stramondo, S. , M. Tesauro, P. Briole, E. Sansosti, S. Salvi, R. Lanari, M. Anzidei, P. Baldi, G. Fornaro, A. Avallone, M. F. Buongiorno, G. Franceschetti and E. Boschi, 1999. The September 26, 1997 Colfiorito, Italy, Earthquakes: Modeled Coseismic Surface Displacement from SAR Interferometry and GPS. *Geophysical Research Letters*, Vol. 26 (No. 7): 883-886.

Strang, G. , 1988. *Linear algebra and its appications*, Orlando, FL: Harcourt Brace Jovanovich Pubblisher.

Tarayare, H. and D. Massonnet, 1996. Atmospheric propagation heterogeneities revealed by ERS-1 interferometry, *Geophysical Research Letters*, Vol. 23: 989-992.

Tesauro, M. , P. Berardino, R. Lanari, E. Sansosti, G. Fornaro and G. Franceschetti, 2000. Urban Subsidence inside the city of Napoli (Italy) observed by satellite radar interferometry. *Geophysical Research Letters*, Vol. 27 (No. 13): 1961-1964.

Usai, S. and R. Klees, 1999. SAR interferometry on a very long time scale: a study of the interferometric characteristics of man-made features. *IEEE Transactions on Geoscience and Remote Sensing*. Vol. 37 (No.4): 2118–2123.

Usai, S., 2000. An analysis of the interferometric characteristics of anthropogenic features. *IEEE Transactions on Geoscience and Remote Sensing*, Vol. 38 (No.3): 1491-1497.

Usai, S., 2001. *A New Approach for Long Term Monitoring of Deformations by Differential SAR Interferometry*, PhD Thesis - Delft University Press, The Netherlands,.

Vadon, H. and F. Sigmundsson, 1997. Crustal deformation from 1992 to 1995 at the midatlantic ridge, southwest Iceland, mapped by satellite radar interferometry. *Science*, Vol. 275: 193-197.

Zebker, H. A. , P. A. Rosen, and S. Hensley, 1997. Atmospheric effects in interferometric synthetic aperture radar surface deformation and topographic maps. *Journal of Geophysical Research*, Vol. 102: 7547-7563.